

## Isothermal compression of face-centered cubic iron

YU NISHIHARA,<sup>1,2,3,\*</sup> YOICHI NAKAJIMA,<sup>1,4</sup> AKIHIKO AKASHI,<sup>1</sup> NORIYOSHI TSUJINO,<sup>1</sup>  
EIICHI TAKAHASHI,<sup>1</sup> KEN-ICHI FUNAKOSHI,<sup>5</sup> AND YUJI HIGO<sup>5</sup>

<sup>1</sup>Department of Earth and Planetary Sciences, Tokyo Institute of Technology, 2-12-1 Ookayama, Meguro, Tokyo 152-8551, Japan

<sup>2</sup>Senior Research Fellow Center, Ehime-University, 2-5 Bunkyo-cho, Matsuyama, Ehime 790-8577, Japan

<sup>3</sup>Geodynamics Research Center, Ehime-University, 2-5 Bunkyo-cho, Matsuyama, Ehime 790-8577, Japan

<sup>4</sup>Bayerisches Geoinstitut, Universität Bayreuth, D-95440 Bayreuth, Germany

<sup>5</sup>Japan Synchrotron Radiation Institute, 1-1-1 Koto, Sayo, Hyogo 679-5198, Japan

### ABSTRACT

Isothermal compression curves of face-centered cubic iron ( $\gamma$ -Fe) were determined at high temperatures (1273 and 1073 K) up to 27 GPa by in situ X-ray diffraction experiments using synchrotron radiation and the Kawai-type multi-anvil apparatus. Fits of the third-order Birch-Murnaghan equation of state to pressure-volume data yielded  $V_0 = 48.997 \pm 0.040 \text{ \AA}^3$ ,  $K_{T0} = 108.3 \pm 2.4 \text{ GPa}$ , and  $K'_T = 5.8 \pm 0.2$  for 1273 K, and  $V_0 = 48.600 \pm 0.098 \text{ \AA}^3$ ,  $K_{T0} = 88.9 \pm 5.1 \text{ GPa}$ , and  $K'_T = 8.9 \pm 0.7$  for 1073 K, where  $V_0$ ,  $K_{T0}$ , and  $K'_T$  are unit-cell volume, bulk modulus and its pressure derivative, respectively, at ambient pressure. The relatively large values of  $K'_T$  are attributable to successive electronic spin state transitions from mixed-spin at lower pressures to low-spin at higher pressures. When discussing the constituents of Earth's (or other planets') solid inner core in terms of density and equations of state, one must carefully consider the influence of the electronic spin state.

**Keywords:** Face-centered cubic (fcc) iron, compression curve, high pressure, spin transition, inner core

### INTRODUCTION

Although it is widely accepted that the Earth's inner core consists of iron with a minor amount of nickel and light elements, its crystal structure remains controversial. The hexagonal-close-packed phase of iron ( $\epsilon$ -Fe) has been considered to be the most probable candidate for the major phase in the inner core primarily based on experimental studies at high-pressure and high-temperature conditions (e.g., Li and Fei 2005; Tateno et al. 2010). On the other hand, some experimental and theoretical studies showed that the face-centered cubic (fcc) phase of iron ( $\gamma$ -Fe) is also a possible candidate as the major constituent of the Earth's inner core (Mikhaylushkin et al. 2007; Kuwayama et al. 2008; Vočadlo et al. 2008).  $\gamma$ -Fe is also expected to be stable under pressure and temperature conditions of the cores of Mercury (e.g., Rivoldini et al. 2009) and Mars (e.g., Gudkova and Zharkov 2004). Therefore, the knowledge of the physical properties of  $\gamma$ -Fe at high pressure and high temperature is important to understand the nature of the metallic cores of the Earth and other planets.

At ambient pressure,  $\gamma$ -Fe is characterized by unusually high thermal expansion which is called "anti-Invar" behavior (e.g., Acet et al. 1994; Wassermann and Acet 2005). Invar, which is characterized by very small thermal expansion, and anti-Invar behavior have been found in many 3d element-based metals with fcc structure. Several models have been proposed to explain Invar and anti-Invar behavior (Wassermann 1990). The 2- $\gamma$  state model is one of the most well-known hypotheses where the very high thermal expansion in anti-Invar is due to the gradual change in occupancy of electronic spin states (e.g., Moruzzi 1990). This spin transition proposed by the 2- $\gamma$  state model may also have a significant

influence on the thermoelastic behavior of  $\gamma$ -Fe at high-pressure and high-temperature conditions corresponding to the Earth's and planetary interiors. Although pressure-volume-temperature ( $P$ - $V$ - $T$ ) measurements of  $\gamma$ -Fe were reported in several previous studies (Boehler et al. 1989, 1990; Funamori et al. 1996; Campbell et al. 2009; Komabayashi and Fei 2010), none of these studies made isothermal compression experiments. A systematic study on the compression behavior of  $\gamma$ -Fe is needed to examine the influence of the electronic spin state at high pressure. In this paper, we report new isothermal compression data of  $\gamma$ -Fe at 1273 and 1073 K up to 27 GPa and discuss the influence of the spin transition on its thermoelastic behavior.

### EXPERIMENTAL METHODS

High-temperature compression experiments were conducted using a Kawai-type multi-anvil apparatus, SPEED-Mk II, installed at the synchrotron beamline BL04B1 at the SPring-8 synchrotron facility, Japan (Katsura et al. 2004). The 14M/8 (where 14M stands for octahedral pressure medium of 14.0 mm edge length and 8 stands for 8.0 mm truncation of the tungsten-carbide anvils) and 8M/3 cell assemblies were used for the experiments in run M605 and runs M620 and M622, respectively. The sample was heated with a cylindrical graphite (14M/8) or TiB<sub>2</sub> + hBN composite (8M/3) furnace embedded in a pressure medium made of MgO doped with 5 wt% Cr<sub>2</sub>O<sub>3</sub>, and the temperature was measured using a W5%Re-W26%Re thermocouple (Fig. 1). The grooves made for the thermocouple path were filled with Al<sub>2</sub>O<sub>3</sub> cement.

The reagent of Fe powder sample (99.998% purity, Newmet Koch) was mixed with MgO powder (99.9% purity, Wako Pure Chemical Industries) to inhibit grain growth during high-temperature compression experiments [Fe:MgO = 21:79 (M605), 30:70 (M620, M622) in volume ratio]. During the beginning stages of this study, hBN powder was mixed with the Fe sample; however, this yielded significant contamination of the sample with nitrogen during experiments. Thus, MgO was mixed in later experiments because the composition of the Fe sample itself does not change during experiments although (Mg,Fe)O is formed by the reaction of Fe, MgO, and oxygen with air. Since contamination with hydrogen has significant influence on the unit-cell volume of  $\gamma$ -Fe at high pressure (e.g., Fukai 2005; Sakamaki et al. 2009), it is critically important to remove water from the sample and cell assembly prior to

\* E-mail: yunishi@sci.ehime-u.ac.jp

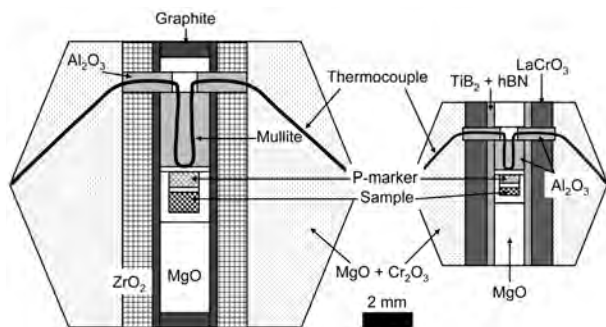


**FIGURE 1.** Schematic cross section of cell assemblies used (a) in M605 (14M/8 assembly), and (b) in M620 and M622 (8M/3 assembly). Along X-ray paths, materials were replaced by B + Epoxy to maximize X-ray flux.

experiments. The mixture of Fe sample and MgO was pelletized to rods and subsequently heated at 1270 K for 1–5 min under relatively reducing conditions ( $\log f_{O_2} \sim IW+0.6$  where IW is the iron-wüstite buffer) in order to completely remove volatiles from the sample. Similarly, the MgO pressure marker was mixed with 10 wt% Pt to prevent significant grain growth at high temperature, pelletized, and then heated at 1270 K. Both the sample and the pressure marker were contained in an MgO capsule and separated by an MgO disk (Fig. 1). The assembled cells were dried at 380 K for more than one night before experiments.

The X-ray diffraction measurements were carried out by the energy-dispersive method at a fixed  $2\theta$  angle of  $\sim 8.0^\circ$  using white synchrotron X-rays and a Ge solid-state detector connected to a multi-channel analyzer. The other details of the X-ray diffraction system are the same as those described in Akashi et al. (2009). Typical exposure time for collecting each diffraction pattern of the sample and the pressure marker was 200–300 s. Figure 2 shows a diffraction pattern of  $\gamma$ -Fe. The unit-cell volume of  $\gamma$ -Fe was calculated typically from 3 diffraction peaks (111, 200, and 311). Pressure was determined using the unit-cell volume of MgO in the pressure marker, which was calculated using 5 diffraction peaks (111, 200, 220, 311, and 222) and the equation of state of MgO by Matsui et al. (2000). The diffraction data of MgO mixed with the Fe sample were not used in pressure determination because it reacted to form (Mg,Fe)O as described above. The sample was first compressed to 1–8 GPa at room temperature and then heated to 1273 or 1073 K. With fixed temperature, pressure was increased to each target pressure with an increasing rate of  $\sim 0.02$ – $0.3$  GPa/min, and then diffraction data were collected (Fig. 3).

## RESULTS AND DISCUSSION

Figure 3 shows pressure-temperature conditions for the present experiments and observed phases at corresponding conditions. In all three experiments, the  $\alpha$ -phase (body-centered cubic phase)

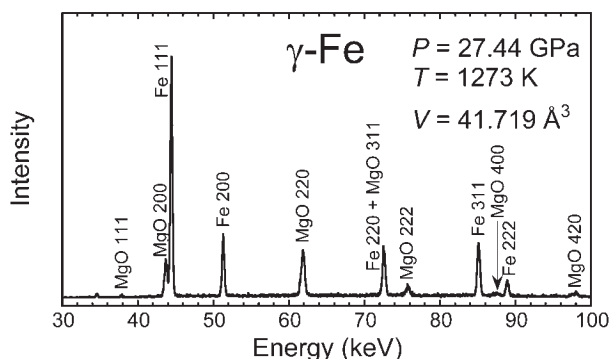


**FIGURE 2.** X-ray diffraction pattern of sample at a pressure of 27.44 GPa and temperature of 1273 K. Diffraction peaks from  $\gamma$ -Fe and MgO [(Mg,Fe)O] are observed. Exact value of diffraction angle for the pattern is  $2\theta = 7.98406^\circ$ .

of Fe transformed to the  $\gamma$ -phase during the first heating to target temperatures. In the experiments at 1273 K, no further phase transformation was observed during subsequent compression up to 27 GPa (M605, M620). On the other hand, during compression at 1073 K, the  $\epsilon$ -phase (hexagonal-close-packed structure) appeared at 22.4 GPa. The observed phase relationship is consistent with previous studies (Bundy 1965; Funamori et al. 1996).  $P$ - $V$  data of  $\gamma$ -Fe were taken during nearly the entire pressure range of the  $\gamma$ -Fe stability field at 1073 and 1273 K.

The  $P$ - $V$  data at 1273 and 1073 K are shown in Table 1 and Figure 4a. The unit-cell volume of  $\gamma$ -Fe at constant temperature decreased monotonically with increasing pressure. The fits of the third-order Birch-Murnaghan equation of state (e.g., Birch 1952) to isothermal compression data yielded  $V_0 = 48.997 \pm 0.040 \text{ \AA}^3$ ,  $K_{T0} = 108.3 \pm 2.4 \text{ GPa}$ , and  $K'_T = 5.8 \pm 0.2$  for 1273 K, and  $V_0 = 48.600 \pm 0.098 \text{ \AA}^3$ ,  $K_{T0} = 88.9 \pm 5.1 \text{ GPa}$ , and  $K'_T = 8.9 \pm 0.7$  for 1073 K, where  $V_0$ ,  $K_{T0}$ , and  $K'_T$  are unit-cell volume, bulk modulus, and its pressure derivative, respectively, at ambient pressure.

The recovered samples were analyzed by electron microprobe. The formation of (Mg,Fe)O was confirmed in the Fe+MgO mixture, and its chemical composition was  $(\text{Mg}_{0.15}\text{Fe}_{0.85})\text{O}$  for the most iron-rich case (S605). On the other hand, we did not observe any evidence of a change in chemical composition of the Fe sample or that of the MgO pressure marker. This observation is consistent with the very low solubility of oxygen in  $\gamma$ -Fe reported by previous studies (Ringwood and Hibberson 1990; Seagle et al. 2008). Therefore, we conclude that our  $P$ - $V$  data of  $\gamma$ -Fe are not affected by a chemical change of the sample or pressure marker.

Figure 4b shows comparisons of the  $P$ - $V$  relationship of  $\gamma$ -Fe at 1273 K determined in this study with those of the previous studies. The data derived in this study are consistent with data by Basisnki et al. (1955) at 0.1 MPa and by Funamori et al.'s (1996) multi-anvil experiments at 24–26 GPa. Boehler et al. (1989, 1990) and Komabayashi and Fei (2010) carried out  $P$ - $V$ - $T$  measurements of  $\gamma$ -Fe at 5–42 and 21–69 GPa, respectively, using the diamond-anvil cells. Campbell et al. (2009) collected  $P$ - $V$ - $T$  data of  $\gamma$ -Fe using both multi-anvil apparatus and diamond-anvil cells at 4–26 GPa.

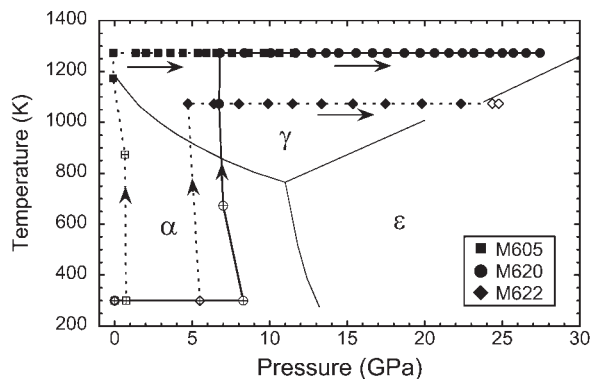


**FIGURE 3.** Pressure and temperature paths in three series of experiments (M605, M620, and M622) and phase relations in Fe. Solid and open symbols and symbols with cross denote  $\gamma$ -phase,  $\epsilon$ -phase, and  $\alpha$ -phase, respectively. In M622,  $\gamma$ - and  $\epsilon$ -phases coexisted at 22.4 GPa and 1073 K due to sluggish transformation kinetics, and the stable phase at this condition is judged to be the  $\epsilon$ -phase. Thin solid lines are previously reported phase boundaries of Fe by Bundy (1965) (below 20 GPa) and Funamori et al. (1996) (above 23 GPa).

**TABLE 1.** *P-V-T* data of  $\gamma$ -Fe

<i>P</i> (GPa)	<i>T</i> (K)	<i>V</i> (Å <sup>3</sup> )
<b>M605</b>		
-0.09(1)	1273	49.030(8)*
1.35(1)	1273	48.421(19)
2.02(3)	1273	48.152(21)
2.80(4)	1273	47.799(12)†
3.60(3)	1273	47.573(2)
4.41(4)	1273	47.282(5)
5.37(2)	1273	46.905(8)
5.93(1)	1273	46.714(7)
6.55(4)	1273	46.489(35)
7.58(2)	1273	46.177(6)
8.66(3)	1273	45.833(20)
9.61(3)	1273	45.517(15)
10.64(2)	1273	45.189(16)
11.57(3)	1273	44.908(11)
<b>M620</b>		
6.81(3)	1273	46.469(11)
8.36(4)	1273	45.991(15)
10.08(2)	1273	45.478(19)
11.66(2)	1273	45.013(21)
12.71(3)	1273	44.759(19)
13.63(3)	1273	44.545(12)
14.45(2)	1273	44.328(17)
15.58(3)	1273	44.095(10)
16.63(6)	1273	43.875(14)
17.59(2)	1273	43.654(13)
18.69(3)	1273	43.400(16)
19.70(4)	1273	43.193(17)
20.64(10)	1273	43.005(19)
21.57(10)	1273	42.817(17)
22.44(12)	1273	42.661(12)
23.17(6)	1273	42.495(11)
24.19(6)	1273	42.323(8)
25.01(3)	1273	42.147(9)
25.72(2)	1273	42.024(3)
26.55(3)	1273	41.875(16)
27.44(10)	1273	41.719(12)
<b>M622</b>		
4.73(3)	1073	46.481(10)
6.41(7)	1073	45.936(14)
8.02(2)	1073	45.460(18)
9.90(3)	1073	44.931(21)
11.48(2)	1073	44.500(19)
13.36(1)	1073	44.037(24)
15.37(2)	1073	43.581(19)
17.47(4)	1073	43.151(15)
19.82(7)	1073	42.699(16)
22.34(7)	1073	42.277(20)
24.37(4)	1073	41.948‡

Notes: Pressures were calculated using equation of state of MgO by Matsui et al. (2000). Numbers in parentheses denotes the errors in the last digits.

\* Diffraction peak (111) is not used.

† Diffraction peak (200) is not used.

‡ Only diffraction peak (200) is used.

At a relatively low pressure region ( $P < \sim 10$  GPa), equations of state of Campbell et al. (2009) and Komabayashi and Fei (2010) exhibit larger and smaller volumes, respectively, compared to our results, and converge on a similar value at higher pressure ( $P > \sim 25$  GPa). This could be partly due to lack of data at relatively low pressures in these previous studies. On the other hand, the equation of state by Boehler et al. (1989, 1990) yielded a comparatively smaller volume at higher pressures ( $P > \sim 10$  GPa), which might be due to less accurate temperature and pressure control at that time. Sakamaki et al. (2009) derived the equation of state of  $\gamma$ -Fe using data by Basinski et al. (1955) and Funamori et al. (1996) combined with thermoelastic parameters at 0.1 MPa by Zaretsky and Stassis (1987) and Osetsky and Serra (1998). Our results show good agreement with Sakamaki et al.'s (2009) equation of state. In summary, our results are generally consistent with previous data at 0.1 MPa and recent data obtained by multi-anvil

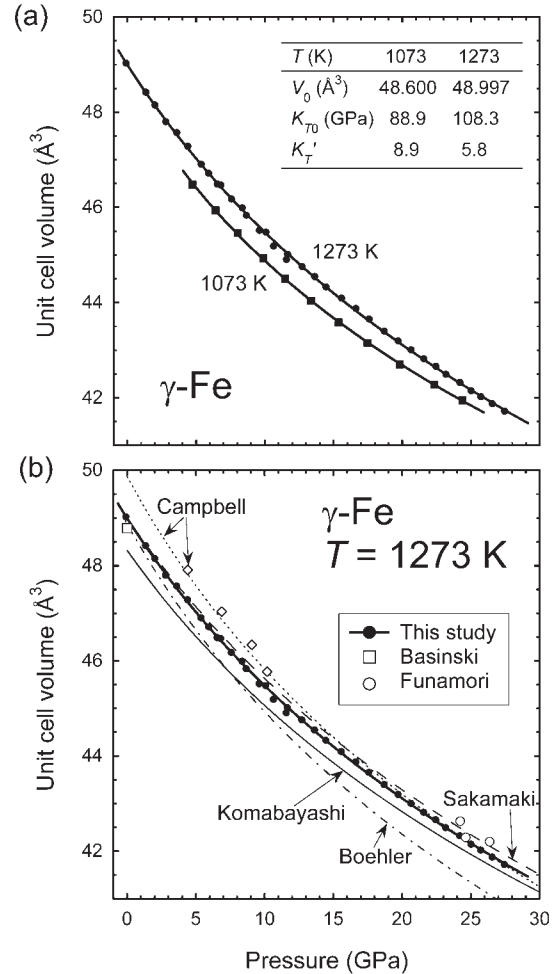


**FIGURE 4.** Compression curves of  $\gamma$ -Fe. (a) Data derived in this study at 1273 K (circles) and 1073 K (squares) with fits of third-order Birch-Murnaghan equation of state. (b) Comparison with previous studies (Basinski et al. 1955; Boehler et al. 1989, 1990; Funamori et al. 1996; Sakamaki et al. 2009; Campbell et al. 2009; Komabayashi and Fei 2010) at 1273 K. The plotted data of Funamori et al. (1996) were derived by interpolation of data taken at temperatures close to 1273 K. For these comparisons, the compression curves of previous studies were calculated using the same methods as in the original references except for that of Boehler et al. (1989, 1990), which was calculated based on a fit of the high-temperature Birch-Murnaghan equation of state (e.g., Nishihara et al. 2005) to the original *P-V-T* data.

and DAC experiments.

The pressure derivative of the bulk modulus at ambient pressure ( $K_T'$ ) determined in this study was relatively high especially at 1073 K ( $K_T' = 8.9$ ), whereas the  $K_T'$  value of most solid metals is in a range of 3–6 (e.g., Raju et al. 1997; Dewaele et al. 2004) and  $K_T'$  of nonmagnetic  $\gamma$ -Fe at 0 K was reported to be 4.4 and 4.3 based on theoretical calculations (Stixrude et al. 1994; Tsuchiya and Fujibuchi 2009). The large  $K_T'$  values in this study could be due to an electronic spin transition in  $\gamma$ -Fe during compression. The  $\gamma$ -Fe at 0.1 MPa is known as “anti-Invar,” which is characterized by a large thermal expansion coefficient (e.g., Acet et al. 1994; Wassermann and Acet 2005). In some literatures, the high thermal expansion of  $\gamma$ -Fe was explained by a successive elec-

tronic transition from a small-volume low-spin (LS) state at lower temperature to a mixed-spin (MS) state in which a large-volume high-spin (HS) state coexists with an LS state (2- $\gamma$  state model) (e.g., Moruzzi 1990). Since the fraction of the HS state increases continuously with temperature, the apparent thermal expansion of  $\gamma$ -Fe includes the effect of the spin transition as well as the usual lattice expansion. It is reasonable to consider that back-transition occurs with increasing pressure under the MS state where the fraction of the HS state decreases continuously. When this occurs, the sample in the mixed spin state will become less compressible as the fraction of the HS state decreases, until the transition is complete, and the fraction of the HS state is nearly zero. Assuming that the successive spin transition completes within the pressure range of the present experiments, the apparent value of  $K'_T$  should be larger than normal because, in reality, the compression curve should consist of an MS part (more compressible) and an LS part (less compressible). The  $K'_T$  value at 1273 K was smaller than that at 1073 K, which is reasonably explained by the pressure range of the spin transition spreading more at higher temperature due to the thermal excitation of the MS state. Even though the above discussion is not conclusive, it should be noted that a fit function based on the 2- $\gamma$  state model successfully expresses the anomalous compression behavior of Invar alloys (face-centered cubic phase of  $\text{Fe}_{64}\text{Ni}_{36}$  and  $\text{Fe}_{72}\text{Pt}_{28}$ ) in Nataf et al. (2006).

Because of the influence of successive spin transition in  $\gamma$ -Fe at  $P$ - $T$  conditions of this study, direct extrapolation of the present equation of state to higher pressures would yield erroneous results. When the components of the Earth's and planets' cores are discussed in terms of their density and the equations of state, the influence of the electronic spin state should be considered carefully. In order for more accurate understanding of metallic cores, further experimental studies on  $P$ - $V$ - $T$  equation of state of  $\gamma$ -Fe and spin state in Fe at higher pressure and higher temperature conditions are required.

#### ACKNOWLEDGMENTS

We thank T. Imai and Y. Tange for their helpful support during the in situ X-ray diffraction experiments, and T. Suzuki, T. Tsuchiya, and Y. Kuwayama for discussion. We thank S. Whitaker for English editing and improvements. Comments by H. Watson and an anonymous reviewer were helpful for improving the manuscript. The experiments were performed by using the SPEED-Mk.II system at BL04B1 at SPring-8 (proposal no. 2007B1312 and 2007B1246). This work is supported by Grant-in-aid for Young Scientists (B) 17740348 and 20740307 to Y.N. and Scientific Research (A) 18204050 to E.T.

#### REFERENCES CITED

- Acet, M., Záhres, H., and Wassermann, E.F. (1994) High-temperature moment-volume instability and anti-Invar of  $\gamma$ -Fe. *Physical Review B*, 49, 6012–6017.
- Akashi, A., Nishihara, Y., Takahashi, E., Nakajima, Y., Tange, Y., and Funakoshi, K. (2009) Orthoenstatite/clinoenstatite phase transformation in  $\text{MgSiO}_3$  at high-pressure and high-temperature determined by in situ X-ray diffraction: Implications for nature of the X discontinuity. *Journal of Geophysical Research*, 114, B04206, doi:10.1029/2008JB005894.
- Basinski, Z.S., Hume-Rothery, W., and Sutton, A.L. (1955) The lattice expansion of iron. *Proceedings of the Royal Society A*, 229, 459–467.
- Birch, F. (1952) Elasticity and constitution of the Earth interior. *Journal of Geophysical Research*, 57, 227–286.
- Boehler, R., Besson, J.M., Nicol, M., Nielsen, M., Itie, J.P., Weill, G., Johnson, S., and Grey, F. (1989) X-ray diffraction of  $\gamma$ -Fe at high pressures and temperatures. *Journal of Applied Physics*, 65, 1795–1797.
- Boehler, R., von Bargen, N., and Chopelas, A. (1990) Melting, thermal expansion, and phase transitions of iron at high pressures. *Journal of Geophysical Research*, 95, 21731–21736.
- Bundy, F.P. (1965) Pressure-temperature phase diagram of iron to 200 kbar, 900°C. *Journal of Applied Physics*, 36, 616–620.
- Campbell, A., Danielson, L., Righter, K., Seagle, C.T., Wang, Y., and Prakapenka, V. (2009) High pressure effects on the iron-iron oxide and nickel-nickel oxide oxygen fugacity buffers. *Earth and Planetary Science Letters*, 286, 556–564.
- Dewaele, A., Loubeyre, P., and Mezouar, M. (2004) Equations of state of six metals above 94 GPa. *Physical Review B*, 70, 094112.
- Fukai, Y. (2005) *The Metal-Hydrogen System: Basic Bulk Properties*, 400 p. Springer, Berlin.
- Funamori, N., Yagi, T., and Uchida, T. (1996) High-pressure and high-temperature in situ X-ray diffraction study of iron to above 30 GPa using MA8-type apparatus. *Geophysical Research Letters*, 23, 953–956.
- Gudkova, T.V. and Zharkov, V.N. (2004) Mars: interior structure and excitation of free oscillations. *Physics of the Earth and Planetary Interiors*, 142, 1–22.
- Katsura, T., Funakoshi, K., Kubo, A., Nishiyama, N., Tange, Y., Sueda, Y., Kubo, T., and Utsumi, W. (2004) A large-volume high-pressure and high-temperature apparatus for in situ X-ray observation, 'SPEED-Mk. II'. *Physics of the Earth and Planetary Interiors*, 143–144, 497–506.
- Komabayashi, T. and Fei, Y. (2010) Internally consistent thermodynamic database for iron to the Earth's core conditions. *Journal of Geophysical Research*, 115, B03202, doi:10.1029/2009JB006442.
- Kuwayama, Y., Hirose, K., Sata, N., and Ohishi, Y. (2008) Phase relations of iron-nickel alloys up to 300 GPa: Implications for composition and structure of the Earth's inner core. *Earth and Planetary Science Letters*, 2, 379–385.
- Li, J. and Fei, Y. (2005) Experimental constraints on core composition. In R.W. Carlson, Ed., *The Mantle and Core*, 2, p. 521–546. Treatise on Geochemistry, Elsevier, Amsterdam.
- Matsui, M., Parker, S.C., and Leslie, M. (2000) The MD simulation of the equation of state of  $\text{MgO}$ : Application as a pressure calibration standard at high temperature and high pressure. *American Mineralogist*, 85, 312–316.
- Mikhaylushkin, A.S., Simak, S.I., Dubrovinsky, L., Dubrovinskaya, N., Johansson, B., and Abrikosov, I.A. (2007) Pure iron compressed and heated to extreme conditions. *Physical Review Letters*, 99, 165505.
- Moruzzi, V.L. (1990) High-spin and low-spin states in Invar and related alloys. *Physical Review B*, 41, 6939–6946.
- Nataf, L., Decremps, F., Gauthier, M., and Canny, B. (2006) High-pressure structural study of  $\text{Fe}_{64}\text{Ni}_{36}$  and  $\text{Fe}_{72}\text{Pt}_{28}$  Invar alloys at low-temperature. *Physical Review B*, 74, 184422.
- Nishihara, Y., Nakayama, K., Takahashi, E., Iguchi, T., and Funakoshi, K. (2005) P-V-T equation of state of stishovite to the mantle transition zone conditions. *Physics and Chemistry of Minerals*, 31, 660–670.
- Osetsky, Y.N., and Serra, A. (1998) Computer-simulation study of high-temperature phase stability in iron. *Physical Review B*, 57, 755–763.
- Raju, S., Mohandas, E., and Raghunathan, V.S. (1997) The pressure derivative of bulk modulus of transition metals: an estimation using the method of model potentials and a study of the systematics. *Journal of Physics and Chemistry of Solids*, 58, 1367–1373.
- Ringwood, A.E. and Hiberson, W. (1990) The system Fe-FeO revisited. *Physics and Chemistry of Minerals*, 17, 313–319.
- Rivoldini, A., Van Hoolst, T., and Verhoeven, O. (2009) The structure of Mercury and its core sulfur content. *Icarus*, 201, 12–30.
- Sakamaki, K., Takahashi, E., Nakajima, Y., Nishihara, Y., Funakoshi, K., Suzuki, T., and Fukai, Y. (2009) Melting relation of FeH<sub>2</sub> up to 20 GPa: Implication for the temperature of the Earth's core. *Physics of the Earth and Planetary Interiors*, 174, 192–201.
- Seagle, C.T., Heinz, D.L., Campbell, A.J., Prakapenka, V.B., and Wanless, S.T. (2008) Melting and thermal expansion in the Fe-FeO system at high pressure. *Earth and Planetary Science Letters*, 265, 655–665.
- Stixrude, L., Cohen, R.E., and Singh, D.J. (1994) Iron at high pressure: Linearized-augmented-plane-wave computations in the generalized-gradient approximation. *Physical Review B*, 50, 6442–6445.
- Tateno, S., Hirose, K., Ohishi, Y., and Tatsumi, Y. (2010) The structure of iron in Earth's inner core. *Science*, 330, 359–361.
- Tsuchiya, T. and Fujibuchi, M. (2009) Effects of Si on the elastic properties of Fe at Earth's inner core pressures: First principles study. *Physics of the Earth and Planetary Interiors*, 174, 212–219.
- Vočadlo, L., Wood, I.G., Alfè, D., and Price, G.D. (2008) Ab initio calculations on the free energy and high  $P$ - $T$  elasticity of face-centered-cubic iron. *Earth and Planetary Science Letters*, 268, 444–449.
- Wassermann, E.F. (1990) Invar: Moment-volume instabilities in transition metals and alloys. In K.H.J. Buschow and E.P. Wohlfarth, Eds., *Ferromagnetic Materials*, vol. 5, p. 237–322. Elsevier, Amsterdam.
- Wassermann, E.F. and Acet, M. (2005) Invar and anti-Invar: magnetovolume effects in Fe-based alloys revisited. In A. Planes, L. Mañosa, and A. Saxena, Eds., *Magnetism and Structure in Functional Materials*, p. 177–197. Springer, Berlin.
- Zaretsky, J., and Stassis, C. (1987) Lattice dynamics of  $\gamma$ -Fe. *Physical Review B*, 35, 4500–4502.

MANUSCRIPT RECEIVED JULY 20, 2011

MANUSCRIPT ACCEPTED APRIL 25, 2012

MANUSCRIPT HANDLED BY JENNIFER KUNG